Numerical Study on Wave-induced Beam Ion Prompt Losses in DIII-D Tokamak

Zhichen Feng[1], Jia. Zhu[1], Gou-Yong Fu[1,2],* W. W. Heidbrink[3], and M. A. Van Zeeland[4]

[1]*Institute for Fusion Theory and Simulation and Department of physics, Zhejiang University, Hangzhou 310027, China*

[2]*Princeton Plasma Physics Laboratory, Princeton, New Jersey 08543, USA*

[3]*Department of Physics and Astronomy, University of California Irvine, Irvine, California 92697, USA and*

[4]*General Atomics, San Diego, California 92186, USA*

Abstract

A numerical study is performed on the coherent beam ion prompt losses driven by Alfvén eigenmodes(AE) in DIII-D plasmas using realistic parameters and beam ion deposition profile. The synthetic signal of fast-ion loss detector(FILD) is calculated for a single AE mode. The first harmonic of the calculated FILD signal is linearly proportional to the AE amplitude with the same AE frequency in agreement with the experimental measurement. The calculated second harmonic is proportional to the square of the first harmonic for typical AE amplitudes. The coefficient of the quadratic scaling is found to be sensitive to the AE mode width. The second part of this work considers the AE drive due to coherent prompt loss. It is shown that the loss-induced mode drive is much smaller that the previous estimate and can be ignored for mode stability.

*corresponding author's Email: gyfu@zju.edu.cn

I. INTRODUCTION

Prompt beam ion losses driven by Alfven eigenmodes(AE) were recently observed in DIII-D plasmas heated by neutral beam injection[1–7]. The losses were measured by the Fast Ion Loss Detector (FILD) with high frequency response and were coherent with the Alfvén eigenmodes. It was shown that the coherent losses mainly come from trapped particles whose orbits are close to tokamak wall. These trapped ions are first ionized close to the edge of the plasma and are kicked out radially by the Alfvén modes via wave particle interaction and are then lost to wall within one bounce of the banana orbits. The coherent FILD signals oscillate at the same frequencies of the corresponding AEs while the amplitude of the FILD signals are proportional to those of the AEs. These experimental results of AE-induced prompt losses have been explained successfully by an analytic theory as well as numerical simulation by Zhang et al[8]. It was shown that the AE induces a radial displacement of the banana orbit via the local resonant interaction over the inner leg of the banana orbit which intersects the localized AE mode structure. The calculated radial displacement (about a few centimeters) after one bounce is proportional to the AE amplitude with the same frequency. The local resonance condition is given by:

$$\omega = n\langle\dot{\phi}\rangle - m\langle\dot{\theta}\rangle, \tag{1}$$

where ω is the AE mode frequency, n and m are the toroidal and poloidal mode numbers, and $\langle\dot{\phi}\rangle$ and $\langle\dot{\theta}\rangle$ are the averaged toroidal and poloidal angular velocities over the inner leg of the orbit where particles intersect with the localized AE mode. The width of this local resonance is fairly large for the prompt-lost particles, on order of several bounce frequency, because the interaction time is shorter than one bounce period. These analytic results have been confirmed by numerical simulations and recent experimental results[7].

In this work, a numerical study of AE-induced beam ion losses using the realistic DIII-D experimental geometry, parameters and profiles is performed. First we simulate the synthetic FILD signal of AE-induced losses for a single AE using the realistic neutral beam deposition profile from the TRANSP code[9]. The energetic particle-Alfvén eigenmodes code(EAC)[10] is adapted to simulate the fast ion interaction with AE and resultant losses and associated FILD signal. Both the first and second harmonic of the FILD signal are calculated and compared with the experimental observation. This part of our work is mainly motivated by the recent experimental observation[7] where it was shown that the second harmonic has no clear correlation with the first harmonic. Here the second harmonic of FILD signal is calculated in order to explain this counter-intuitive observation. In the second part of our work, the AE drive due to AE-induced prompt loss is simulated. This is motivated by a recent work[11] where an order of magnitude estimate indicated the drive due to prompt

loss can be significant. This work will give a more accurate evaluation of the drive using realistic parameters and beam ion deposition profile. The EAC code is also used to compute the AE growth rate due to all prompt loss particles.

In Section II, beam ion interaction with AE is studied for a model tokamak equilibrium and an analytic AE mode structure. In Section III, and IV, the DIII-D FILD signal and contribution of prompt loss particle to AE mode drive are calculated at constant neutral beam injection power for realistic experimental parameters and profiles. Conclusions and discussions are given in Section V.

II. SIMULATION OF AE-INDUCED ENERGY CHANGE AFTER ONE BOUNCE

In this section we calculate energy change of trapped beam ions after the localized interaction within one bounce in order to compare with previous work and to understand the simulation results of AE-induced prompt losses shown in the next section. As will be shown later the energy change is proportional to the radial displacement of the particle orbit. Therefore the prompt loss is directly related to the particle energy change as a result of wave particle interaction. The calculation is done by the revised EAC code[10] where the guiding center equations in the EAC code are changed to the gyro-kinetic equations, since the fast ion Larmor radius is comparable to spatial scale of the AE mode structures.

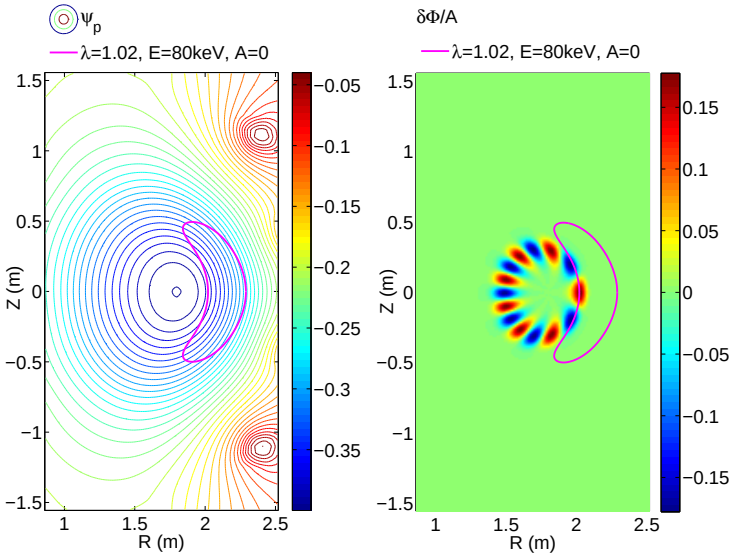

FIG. 1: Poloidal magnetic flux of DIII-D pulse 146096, given perturbed AE electrostatic field normalized by amplitude, and the non-perturbed test particle orbit, where $\lambda = \mu B_0/E$, is the test particle's pitch angle.

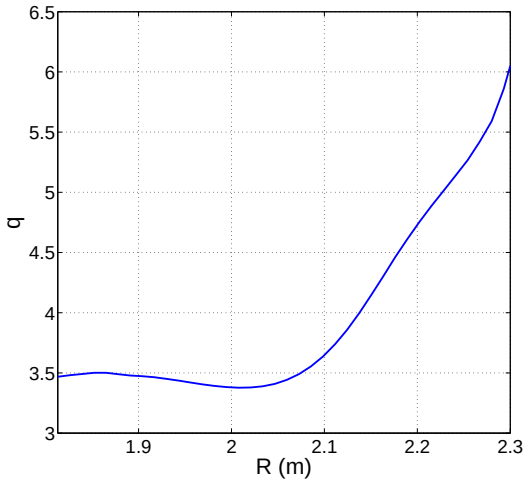

FIG. 2: Safety factor q profile in outer mid plane.

Fig.1 on the left shows the poloidal magnetic flux of DIII-D shot 146096 and a typical trapped particle orbit close to the plasma edge at $R_{edge} = 2.30m$. The wall is located at $R_{wall} = 2.363m$. The major radius of the magnetic axis is $R_0 = 1.80m$, the toroidal magnetic field on axis is $B_0 = 1.94T$. Fig.1 on the right shows the electrostatic potential of a prescribed RSAE and a typical trapped particle orbit with its inner leg intersecting the localized AE mode structure. Fig.2 shows the reversed shear safety factor q profile at outer mid plane with the minimum value about $q_{min} = 3.38$ at $R = 2.03m$ where the RSAE is localized. In this work we use both analytical RSAE mode structure and more realistic AE mode structures obtained from the NOVA code[12] based on realistic equilibrium. The analytic RSAE mode structure, as shown in Fig.1, is prescribed as:

$$\delta\Phi = A\overline{\psi}_p \exp\left[-\left(\frac{\overline{\psi}_p - \overline{\psi}_{q_{min}}}{\Delta}\right)^2\right] \cos\left(-\omega t - (n\phi - m\theta)\right), \tag{2}$$

where A is the amplitude in Volts with the corresponding magnetic perturbation of $\delta B/B_0 \simeq 2 \times 10^{-7}$; $\overline{\psi}_p \equiv (\psi_p - \psi_{p_0})/(\psi_{edge} - \psi_{p_0})$ is the normalized poloidal magnetic flux, ψ_p, ψ_0 and ψ_{edge} are the poloidal magnetic flux at grid point, magnetic axis and plasma edge respectively, and $\overline{\psi}_{q_{min}}$ is the normalized poloidal magnetic flux at the minimum q surface; Δ is the normalized mode width; ω is the real frequency of the mode; ϕ and θ are toroidal and poloidal angle respectively; $n = 2$ and $m = 7$ are toroidal and poloidal mode numbers. This analytical mode structure is similar to the one used in Zhang et al.'s work[8] with $\Delta_0 \sim 0.1$, and $\omega_0 = 6.03 \times 10^5 s^{-1} (f_0 = 96kHz)$.

Fig.3 shows particle energy change after the banana orbit goes through the localized RSAE mode structure versus their initial toroidal angle for several mode amplitudes. The

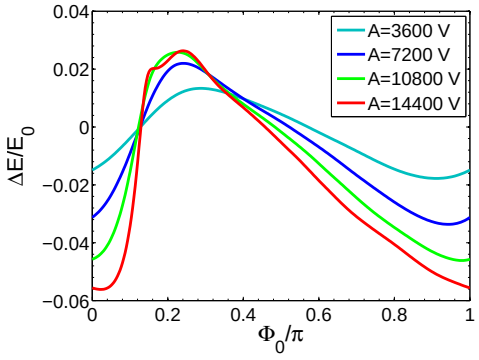

FIG. 3: Test particles' energy change after one bounce VS their initial toroidal angle for different amplitude of AE modes, where $A = 10800V$ corresponding $\delta B_{max}/B_0 = 0.002$.

energy change is naturally a periodic function of toroidal angle with the period the same as mode period. The shape of the function is a distorted sine or cosine. The distortion is due to nonlinear effect since the orbit changes as a result of particle interaction with the RSAE, which leads to the second harmonic of the energy change. The distortion becomes weak as the amplitude decreases as shown later. These results are similar to Zhang's work.

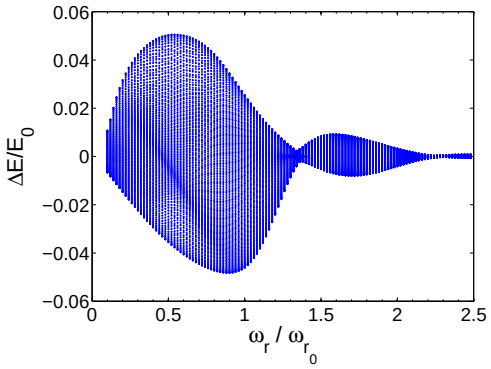

FIG. 4: Test particles' energy change after one bounce VS the frequency of given AEs. Here, when $\omega/\omega_0 = 1$, $\delta B_{max} = 0.0045T$, i.e. $\delta B_{max}/B_0 \approx 0.002$. δB_{max} will be proportional to ω_0/ω_r to keep $E_\parallel = 0$.

Fig.4 shows the test particles' energy change after one bounce versus the frequency of the given AE. Like Zhang's work[8], the resonance frequency width is quite large ($\sim 0.8\omega_0$), which is several bounce frequencies. There is a small second peak near $1.5 \sim 1.7\omega_0$, which may be a higher order local resonance. The envelop of the main peak is similar to Zhang's work.

Fig.5 plots the amplitude ratio of second and first harmonic of test particles' energy change versus wave amplitude. We observe that the ratio is almost linearly proportional to

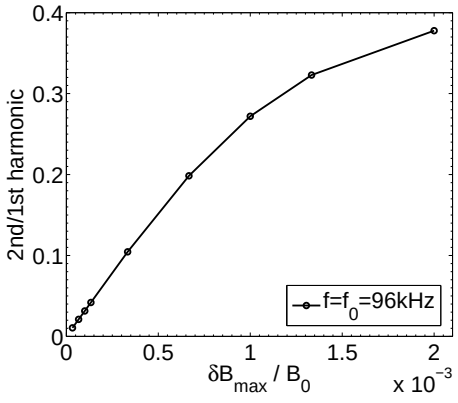

FIG. 5: Intensity ratio of second and first harmonic of test particles' energy change VS wave amplitude.

the amplitude.

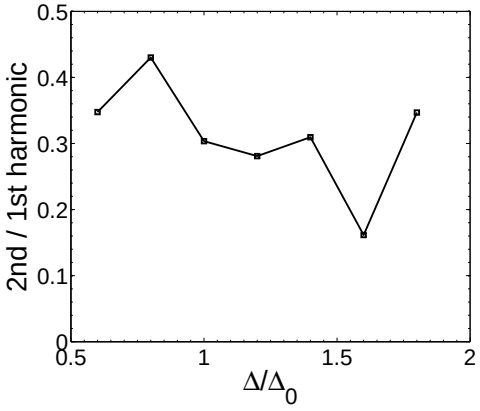

FIG. 6: Intensity ratio of second and first harmonic of test particles' energy change VS wave width.

Fig.6 shows the ratio of δE harmonics as a function of mode width for particles initially located at $R = 2.28m,\ Z = 0$ with $\lambda = 1.0$. This indicates that the size of the second harmonic is sensitive to the mode width.

The above results of test particle energy change due to one-bounce wave particle interaction can be used to understand the results in Section III of the simulated FILD signal because energy change is directly related to the radial displacement of the test particles. According to the canonical Hamiltonian equations, the formula

$$\omega \dot{P}_\phi = n\dot{E} \tag{3}$$

always holds, provided that the given perturbation is a function of $(n\phi - \omega t)$ for a single mode in tokamak[13, 14], where P_ϕ is the canonical toroidal momentum, E is the particle

energy. Note that P_ϕ can be regarded as a radial variable. Thus the energy change is proportional to the radial shift of the orbit, which indicates that the particles move in and out as a result of wave particle interaction. Since the radial shift is directly related to the FILD signal, the first and second harmonics of the energy change correspond to the first and second harmonics of the FILD signal.

III. FILD SIGNAL FROM NEUTRAL BEAM INJECTION

In this section we simulate the FILD signal using realistic neutral beam deposition obtained from the TRANSP code for the DIII-D discharge.

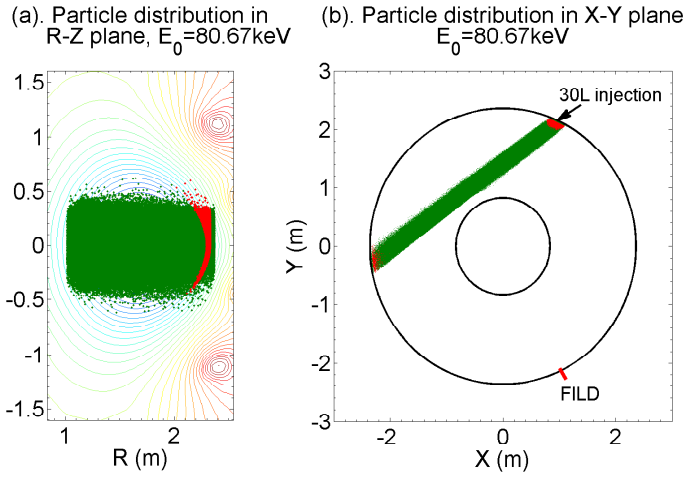

FIG. 7: DIII-D 30L neutral beam injection particle deposition (guiding center) distribution in (a). R-Z plane and (b). X-Y plane. The green points are the deposited particles. The red points are the particles used in our work to calculate the FILD signal and the loss particles' energy change.

Fig.7 plots the DIII-D neutral beam deposition distribution for the 30L beam line in R-Z (one left) and X-Y (on right). Fig.8 plots the same deposition in the λ-P_ϕ phase space where black, green, and blue lines correspond to prompt loss boundary of guiding centers, effective loss boundary due to finite gyroradius, and trapped-passing boundary respectively. The red points are the selected particles for our simulations. These are all trapped particles close to plasma edge whose orbits will intersect AE perturbation before they can be lost to the wall. The green particles left to the red region are lost to wall before they can interact with the AE and are thus not included in our simulations for saving computation time. The FILD's location (R_{FILD}, Z_{FILD}, ϕ_{FILD}) is placed at the same point as it is in DIII-D shot 146096, where $R_{FILD} = 2.36m$, $Z_{FILD} = 0$, $\phi_{FILD} = 4.974rad$. To get a sufficiently large signal

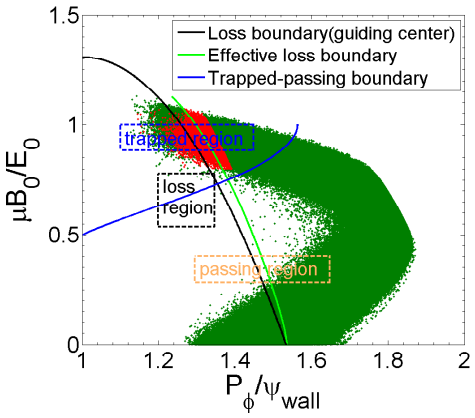

FIG. 8: DIII-D 30L neutral beam injection particle deposition (guiding center) distribution in λ-P_ϕ plane, where $E_0 = 80.67keV$. The effective boundary is the physical boundary minus the particle's Larmor radius.

in numerical calculations, the FILD's window size is enlarged to $\pm 5cm$ in Z and $\pm 0.1rad$ around $\phi = \phi_{FILD}$.

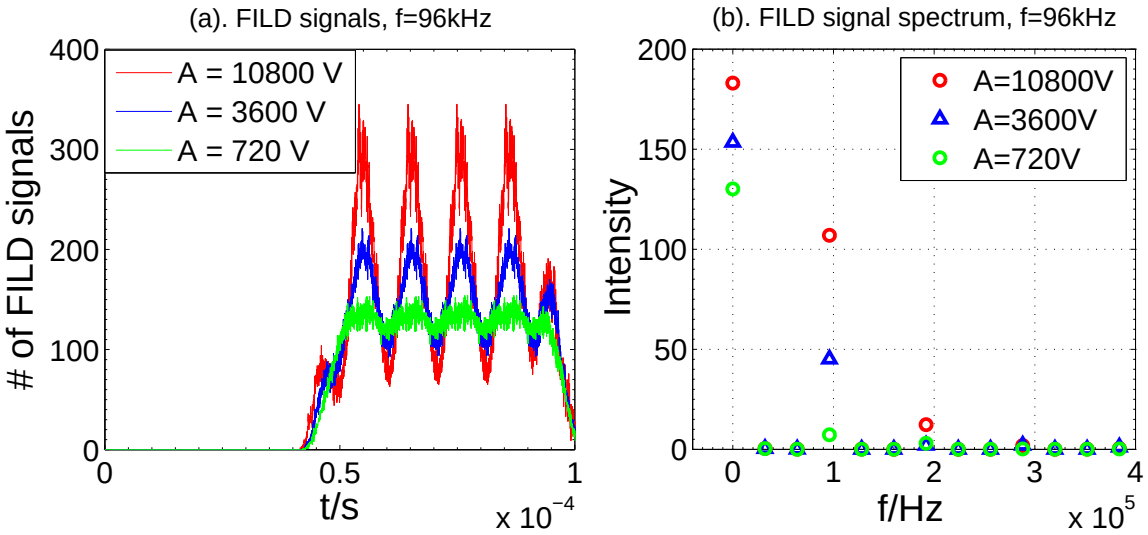

FIG. 9: Real numerical FILD signals and their spectrum. When $A = 10800V$, $\delta B_{max} = 0.0045T$, i.e. $\delta B_{max}/B_0 \approx 0.002$, which is the same as the parameter in Fig.3.

We first calculate the FILD signal for a prescribed analytical AE structure of the n=2 mode. In a wave period $T_p = 10^{-4}s$, the FILD signal is calculated with continuneous injection of the selected particles every two time steps, where the time step in our calculation is $\delta t = T_0/400 = 1/(400f_0) = 2.604 \times 10^{-8}s$. The injection lasts $5 \times 10^{-5}s$, which is about one bounce period of the selected particles. The results are shown in Fig.9(a) for several

mode amplitudes. As expected, the signal oscillates with the mode frequency after the initial transient phase. The signal tends to be constant when the wave amplitude is small (green curve), which corresponds to the intrinsic prompt loss signal from the 30L injected beam. The corresponding spectrum is plotted in Fig.9(b) for several mode amplitudes. It should be noted that the FILD signal is exactly periodic since the AE perturbation has a single frequency. Therefore the spectrum shown is discrete. Fig.10 plots the First harmonic of the FILD signal versus mode amplitude. It is clear that the size of the first harmonic is linearly proportional to the mode amplitude when the mode amplitude is not too large, i.e., when $\delta B_{max}/B_0 < 0.001$.

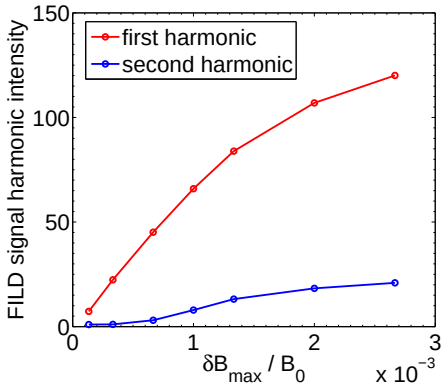

FIG. 10: Intensity of first and second harmonic VS amplitude.

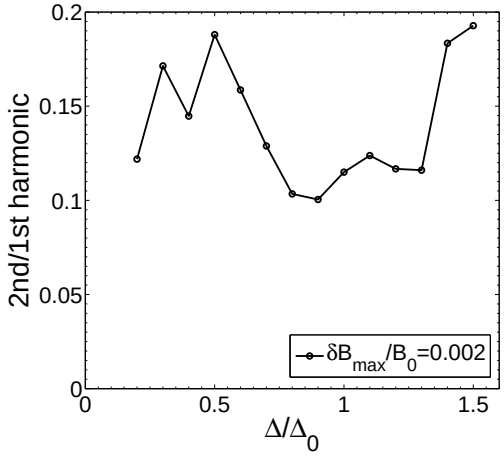

FIG. 11: Ratio of 2nd over 1st harmonic in FILD signal VS mode width.

Fig.11 plots the ratio of the 2nd harmonic over the 1st harmonic of the FILD signal versus the normalized mode width. We observe that the ratio is quite sensitive to the mode width and can vary about a factor of two from 0.1 to 0.2. This result is consistent with the ratio

of harmonics of energy change shown in Fig.6. The sensitivity of the second harmonic to the mode width is presumably due to the complex nonlinearity of the local wave particle interaction. The results of Fig.11 are consistent with the experimental observation [7] where the ratio is measured to be on order of 0.1 and varies a lot.

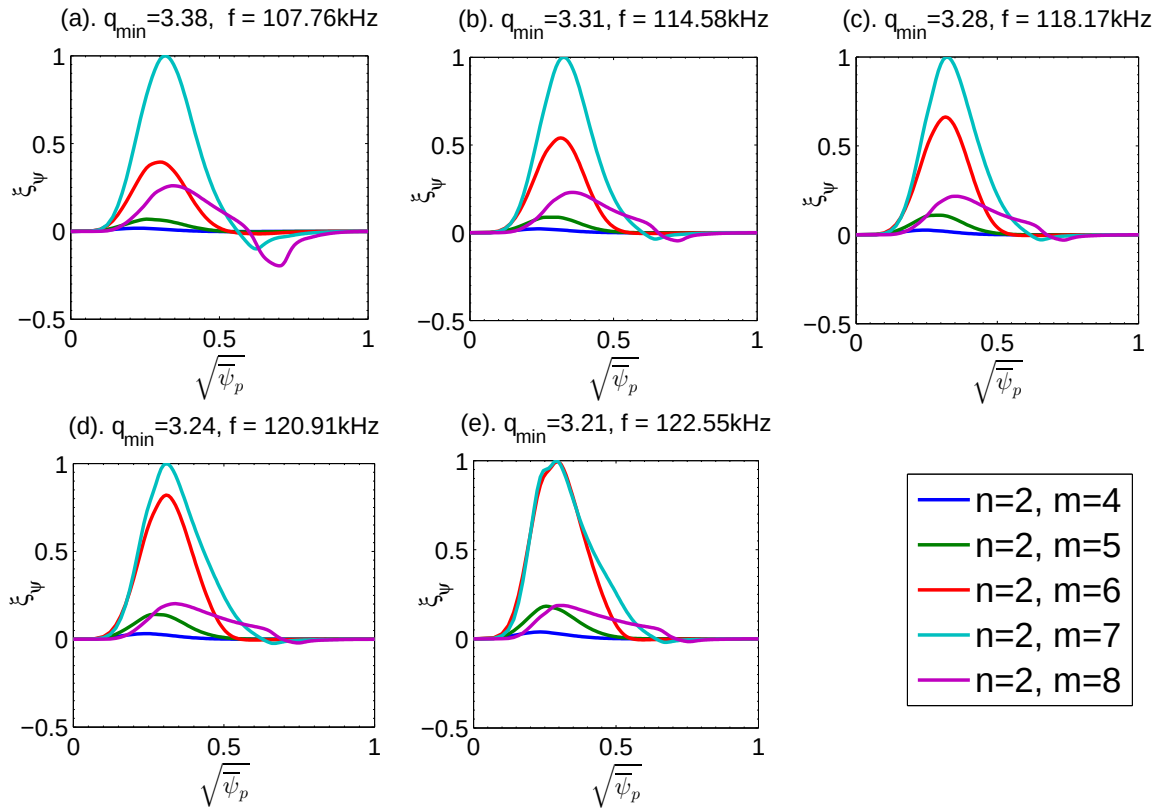

FIG. 12: $n = 2$ AE frequencies and structures for different $q = cq_{original}$ value calculated by NOVA code, where $q_{original}$ is the the original q profile shown in Fig.2, c is a constant factor modifying the q value to change q_{min}, ξ_ψ is defined by $\xi_\psi = \vec{\xi} \cdot \nabla\psi_p$, and $\vec{\xi}$ is the perturbed displacement vector.

We now simulate FILD signal using AE mode structure obtained from the NOVA code in order to be more realistic in comparing the numerical FILD signals with experiment results. Fig.12 shows the $n = 2$ AE frequencies and mode structures obtained using the NOVA code, where we vary q profile by multiplying $q_{original}$(the original q profile shown in Fig.2) with a constant factor c so that $q = cq_{original}$. This factor is used to scan the value of q_{min} in a small range. As expected, when q_{min} becomes smaller, the sideband ($n = 2$, $m = 6$ mode) of the n=2 RSAE[15, 16] increases and the mode frequency also increases. The RSAE eventually becomes a TAE[17] at $q_{min} = 3.25$. NOVA results for n=3 AE modes are similar as shown in Fig.13.

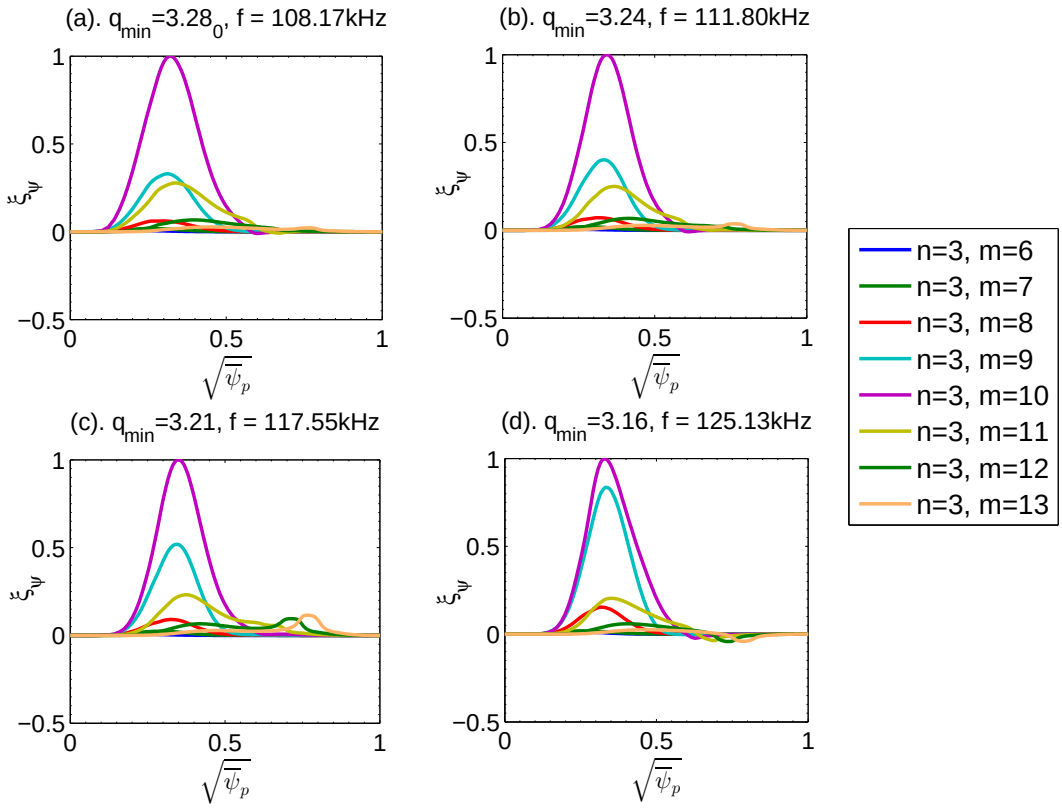

FIG. 13: $n = 3$ AE frequencies and structures for different different $q = cq_{original}$ value calculated by NOVA code, where $q_{original}$ is the the original q profile shown in Fig.2, c is a constant factor modifying the q value to change q_{min}, ξ_ψ is defined by $\xi_\psi = \vec{\xi} \cdot \nabla\psi_p$, and $\vec{\xi}$ is the perturbed displacement vector.

The FILD signal is calculated for several mode amplitudes of $n = 2$ RSAE at $q = q_0$ (The corresponding $n = 2$ mode is shown in Fig.12(a)). Fig.14 plots the first and second harmonic amplitude of FILD signal, and the ratio of second harmonic over first harmonic versus mode amplitude respectively. The results are similar to the results with analytic mode structure shown in Fig.10. In the low amplitude region($B_{max}/B_0 < 0.003$), the amplitude of first harmonic is almost linearly proportional to the mode amplitude, while the second harmonic is approximately quadratic to the amplitude, so that the ratio between them is linear to the amplitude. The results are similar for $n = 3$ RSAE case plotted in Fig.15.

Fig.16 plots the first and second harmonic as well as the ratio as a function of q_{min} for the $n = 2$ AE (see Fig. 12 for the corresponding mode structure and frequency at each q_{min}). We observe that the absolute values and the ratio of these two harmonics change little when q value is varied (the mode width keeps almost the same when q varying). When RSAE changes to TAE as q_{min} decreases, the frequency of the AE increases about 20%, which tend

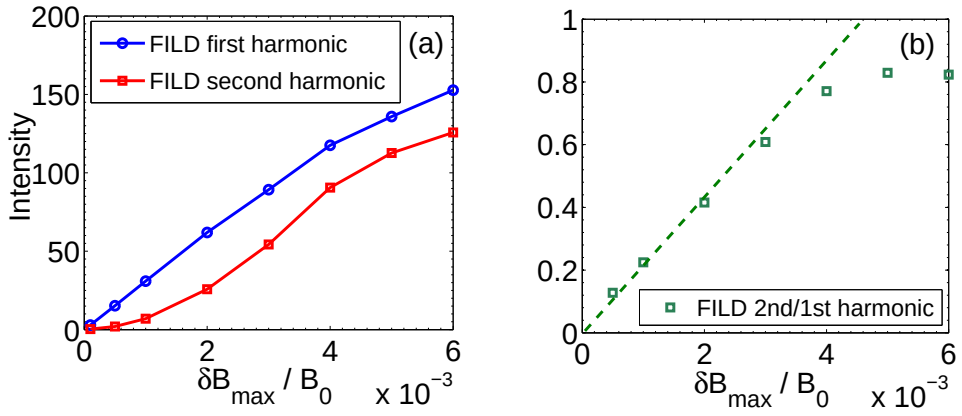

FIG. 14: FILD spectrum (a) first and second harmonic intensities VS wave amplitude, and (b) the ratio of second harmonic over first harmonic VS wave amplitude for $q = q_{original}$, $n = 2$ RSAE case shown in Fig.12(a).

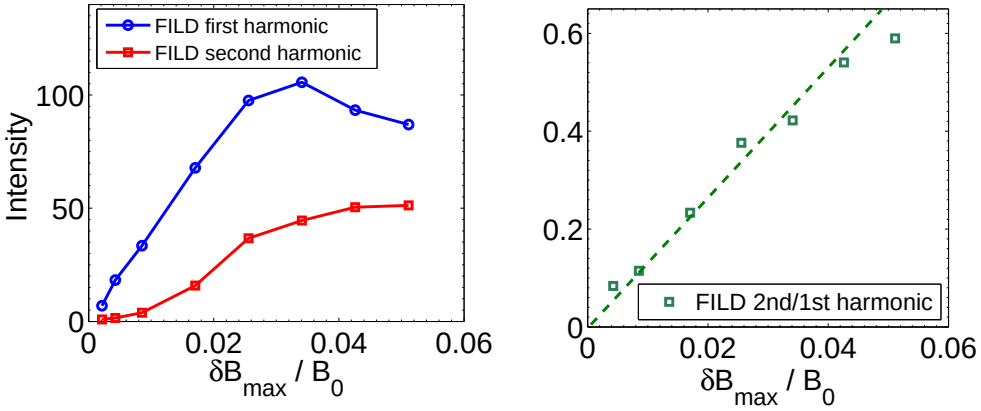

FIG. 15: (a) first and second harmonic intensities VS wave amplitude, and (b) the ratio of second harmonic over first harmonic VS wave amplitude for AE modes shown in Fig.13(a), $q_{min} = 3.28$, $n = 3$ cases.

to make the particles further from the local resonance peak show in Fig.4. On the other hand, the sideband of the RSAE increases when q_{min} decrease as shown in Fig.12 and 13, which may enhance the FILD signal. We believe that these two competing effects tend to cancel so that the FILD signal stays nearly constant as the mode changes. It should be noted that the calculated ratios of second harmonics to the first harmonic based on NOVA mode structure are about a factor of two larger than the corresponding result from the analytic n=2 RSAE and thus are a bit higher than the experimental observed values.

Finally we make an estimate on the size of radial kick of trapped particles due to the local resonant interaction with the AEs. Fig.17 plots the maximum radial displacement of

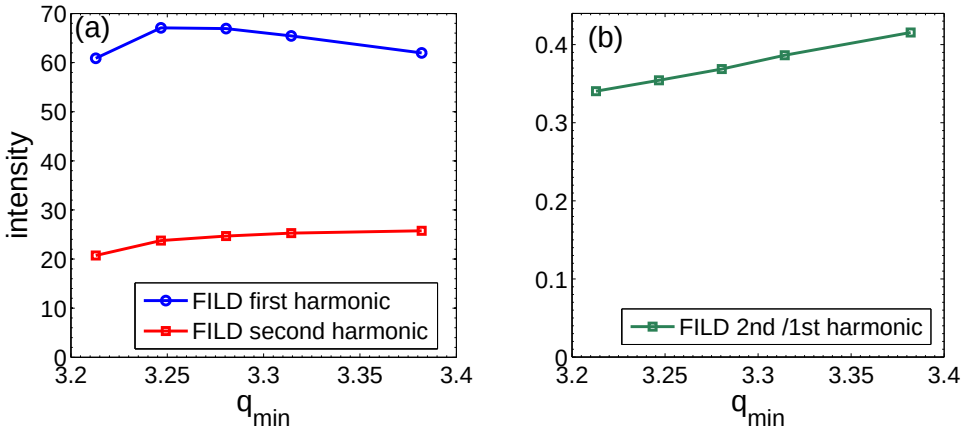

FIG. 16: The first and second harmonic intensities and the ratio of second harmonic over first harmonic VS q value. The $n = 2$ mode structures and frequencies for different q values are show in Fig.12, where amplitude given here is $B_{max}/B_0 = 0.002$.

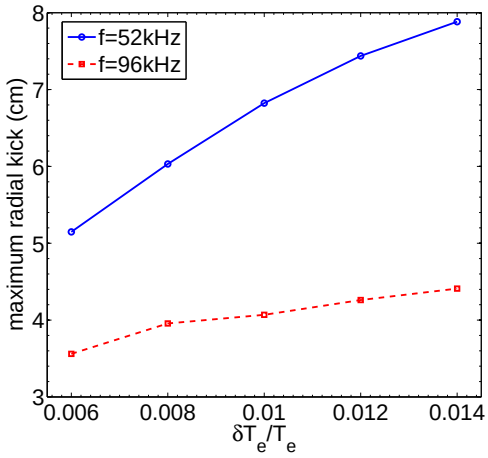

FIG. 17: Maximum radial displacement of 1000 trapped particles after one bounce VS wave amplitude.

1000 trapped particles for two mode frequencies. The particles are located at $R = 2.26m$ on mid plane initially with a pitch angle distribution similar to the experimental deposition. The displacement is measured when a particle crosses the outer mid plane. We find that the maximum displacement for the $f = 52kHz$ AE is larger than that of the $f = 96kHz$ case. This is because the lower frequency is nearer the center of local wave particle resonance. The calculated radial kick size is comparable to the experimental values of $10cm$.

IV. MODE DRIVE DUE TO PROMPT LOSSES

In this section we make a realistic calculation of AE drive due to AE-induced prompt losses. The calculation is more realistic than the previous work since we use experimental beam deposition (based on TRANSP modeling) and DIII-D geometry and parameters. The calculation is based on all of prompt lost particles whether they are seen by FILD or not.

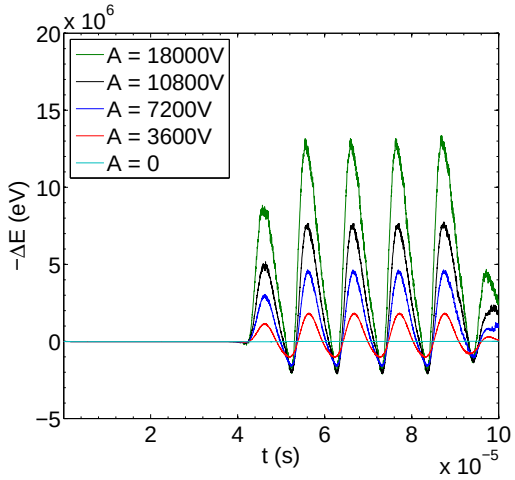

FIG. 18: Time evolution of energy decrease for all loss particles. The $n = 2$, $m = 7$ AE perturbation here is given analytically by Eq.2, with frequency $f = f_0 = 96kHz$.

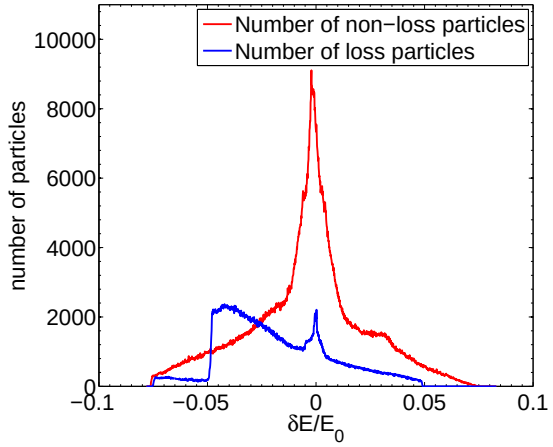

FIG. 19: Energy change distribution for loss particles and non-loss particles, where the energy grid is $10eV/E_0 = 1.24 \times 10^{-4}$, and particles are injected in one wave period. The analytical RSAE perturbation is given by Eq.(2), with $f = 96kHz$, $A = 10800$, or $\delta B_{max}/B_0 \simeq 0.002$.

Fig.18 plots the time evolution of net energy change of all lost particles with analytically

AE perturbation given by Eq.2 for several mode amplitudes. Note that the net energy change is negative for most of time but it is positive (energy gain) for sometimes ($-\Delta E$ value is negative) even when mode amplitude is large. This shows that not all the lost particles lose energy to the wave. This is because there are particles deposited deep in the loss region in Fig.8. These particles would move inward radially for certain mode phase but still remain in loss cone and lost to wall after one bounce. The portion of these particles among all lost particles can be determined from the Fig19, which plots energy change distribution for lost particles and confined particles for all particles injected over one wave period.

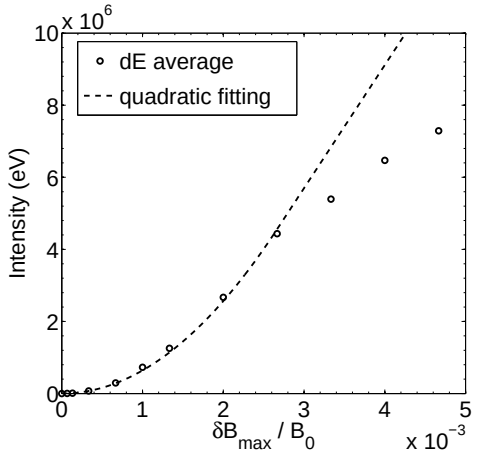

FIG. 20: Average(zeroth harmonic) of energy decrease for all loss particles VS amplitude. The $n = 2$, $m = 7$ AE perturbation here is given analytically in Eq.(2).

Fig.20 plots the time-averaged energy change for all lost particles versus wave amplitude. The averaged energy loss is quadratic in wave amplitude for $\delta B_{max}/B_0 < 2.7^{-3}$.

Following Heidbrink et al[11], the mode drive power or energy loss power can be calculated by:

$$P_{drive} = f_{depo} f_E P_{inj} \tag{4}$$

where P_{inj} is the neutral beam injection power, which is 4.6MW in DIII-D shot 146096, f_{depo} is the fraction of injected beam ions that are lost to wall, and $f_E = \delta E/E_0$ is the averaged fraction of particle energy per lost particle that is delivered to the mode. For the case of Fig.18 and 19 with analytic n=2 RSAE at $\delta B/B_0 \simeq 0.002$, $f_{depo} = 0.42\%$ and $f_E = 1.58\%$. Thus we arrive at:

$$P_{drive} = f_{depo} f_E P_{inj} = 0.0042 \times 0.0158 \times P_{inj} = 305W. \tag{5}$$

Using these numbers, the normalized mode drive can be obtained as:

$$\frac{\gamma}{\omega} = \frac{P_{drive}}{2\omega E_{mode}} = 5.17 \times 10^{-5}, \tag{6}$$

where $E_{mode} = 4.89J$ is the mode energy. We have also calculated the mode drive based on more realistic AE mode structures obtained from the NOVA code. For the case of the n=2 RSAE with $q = q_{original}$ and $\delta B/B_0 \simeq 0.002(\delta T_i/T_i \simeq 0.01)$, the results are $P_{drive} = 69.35W$ and $\gamma/\omega = 1.3 \times 10^{-5}$, which is even smaller because the wave frequency is farther from the peak of local resonance frequency. Compared to the previous estimate of mode drive $\gamma/\omega = 4 \times 10^{-3}$[11], our drive is much lower and can be ignored. The discrepancy mainly comes from the over-estimation of f_{depo} and f_E. Specifically our value of $f_{depo} = 0.42\%$ is about a factor of 5 smaller than the previous estimate of $f_{depo} = 2\%$ and our value of $f_E = 1.58\%$ is a factor of 8 smaller than the previous estimate of $f_E = 13\%$. The overestimation of f_{depo} in the previous work is partly due to the fact that some of the particles near the local resonance may not be lost promptly if they are first kicked inward by the AE. The overestimation of f_E can be explained by the results of Fig. 19 (see blue curve). It is shown there that the energy change of lost particles has a wide distribution in the range of $-0.05 < \delta E/E_0 < 0.05$, i.e., some of the lost particles actually gains energy as explained above. Thus the averaged energy loss per lost particle is smaller.

V. CONCLUSION

In conclusion, a numerical study has been performed on the coherent beam ion prompt losses driven by Alfvén eigenmodes(AE) in DIII-D plasmas using realistic experimental parameters and beam ion deposition profile. The synthetic signal of fast-ion loss detector(FILD) is calculated for a single AE mode. The first harmonic of the calculated FILD signal is found to be linearly proportional to the AE amplitude with the same AE frequency in agreement with analytic theory and the DIII-D experimental measurement. The calculated second harmonic is proportional to the square of the first harmonic for typical experimental AE amplitudes. The amplitude of the second harmonics of the FILD signal is found to scale quadratically with the first harmonic. The size of the second harmonic is found to be sensitive to the mode width. This result can explain partly poor correlation of the second harmonic with the first harmonic. Future work will further explore sensitivity of second harmonic and more generally nonlinear harmonics in the presence of multiple modes. The second part of this work considers the AE drive due to coherent prompt losses. It is shown that the prompt-loss-induced mode drive is much smaller than the previous estimate and can be ignored for mode stability.

Acknowledgments

[1] M. A. Van Zeeland et al., Phys. Plasmas 18, 056114 (2011).

[2] X. Chen, R. K. Fisher, D.C. Pace, M. Garcia-Munoz, J. A. Chavez, W.W. Heidbrink, and M. A. Van Zeeland, Rev. Sci. Instrum. 83, 10D707 (2012).

[3] X. Chen, M. E. Austin, R. K. Fisher, W. W. Heidbrink, G. J. Kramer, R. Nazikian, D. C. Pace, C. C. Petty, and M. A. Van Zeeland, Phys. Rev. Lett. 110, 065004 (2013).

[4] X. Chen, W. W. Heidbrink, G. J. Kramer, M. A. Van Zeeland, M. E. Austin, R. K. Fisher, R. Nazikian, D. C. Pace, and C. C. Petty, Nucl. Fusion 53, 123019 (2013).

[5] X. Chen, W. W. Heidbrink, M. A. Van Zeeland, G. J. Kramer, D. C. Pace, C. C. Petty, M. E. Austin, R. K. Fisher, J. M. Hanson, R. Nazikian, and L. Zeng, Rev. Sci. Instrum. 85, 11E701 (2014).

[6] X. Chen, G.J. Kramer, W.W. Heidbrink, R.K. Fisher, D.C. Pace, C.C. Petty, M. Podesta and M.A. Van Zeeland, Nucl. Fusion 54 083005 (2014).

[7] W. W. Heidbrink, E. A. D. Persico, M. E. Austin, Xi Chen, D. C. Pace and M. A. Van Zeeland, Phys. Plasmas 23, 022503 (2016).

[8] R. B. Zhang, G. Y. Fu, R. B. White, and X. G. Wang, Nucl. Fusion 55 122002 (2015).

[9] R. J. Goldston et al., J. Comput. Phys. 43, 61 (1981).

[10] J. Zhu, G. Y. Fu, and Z. W. Ma, Phys. Plasmas 20, 072508 (2013).

[11] W. W. Heidbrink, Guo-Yong Fu, and M. A. Van Zeeland, Phys. Plasmas 22, 082507 (2015).

[12] C. Z. Cheng and M. S. Chance, J. Comput. Phys. 71, 124 (1987).

[13] R. B. White, The Theory of Toroidally Confined Plasmas, 2nd ed. (Imperial College Press, London, 2001).

[14] R. B. White, N. Gorelenkov, W. W. Heidbrink, and M. A. Van Zeeland, Phys. Plasmas, 17, 056107 (2010).

[15] Y. Kusama, H. Kimura, T. Ozeki, M. Saigusa, G. J. Kramer, T. Oikawa, S. Moriyama, M. Nemoto, T. Fujita, K. Tobita, G. Y. Fu, R. Nazikian, and C. Z. Cheng, Nucl. Fusion 38, 1215 (1998).

[16] S. E. Sharapov, D. Testa, B. Alper, D. N. Borba, A. Fasoli, N. C. Hawkes, R. F. Heeter, M. Mantsinen, M. G. von Hellermann, and EFDA-JET Work-Programme, Phys. Lett. A 289, 127 (2001).

[17] C. Z. Cheng, L. Chen, and M. Chance, Ann. Phys. 161, 21 (1985).